Analytical Methods

PAPER

View Article Online
View Journal | View Issue

Cite this: *Anal. Methods*, 2019, **11**, 5038

Investigation of cavitation-induced damage on PDMS films

Alex H. Wrede,[a] Faisal Al-Masri,[a] Reza Montazami[a] and Nicole N. Hashemi*[ab]

Received 24th July 2019
Accepted 29th August 2019

DOI: 10.1039/c9ay01576k

rsc.li/methods

Traumatic brain injuries (TBIs) are complex phenomena that create epidemic healthcare and financial concerns. Recent studies have theorized that cavitation exists during a TBI and has potential to induce significant damage to the surrounding anatomy. This study seeks to implement polydimethylsiloxane (PDMS) films as a placeholder of the brain to elucidate the damage that the surrounding brain tissue would experience from nearby cavitation. The apparatus includes an existing methodology that implements controlled cavitation. 3D confocal microscopy and interferometry techniques are used to characterize the surface damage to the PDMS films. Visual representation and roughness parameters on the nanoscale help elucidate a distinct difference between control and experimental samples. These results help legitimize the concern of cavitation in the skull and also help motivate future studies to analyze the cellular response to surrounding cavitation.

1. Introduction

Despite decades of research, the brain continues to be one of the most obscure parts of the human body. TBI is the damaging aftermath to the brain due to a mechanical force, leading to functionality impairment. Exposure to blasts has led to TBI in over 60% of soldiers serving in Iraq and Afghanistan.[1] Everyone in society is susceptible to TBI; this diagnosis is typical in falls and automobile collisions. TBIs are also prevalent in contact sports where athletes are often exposed to cranial impacts.[2] There are many different leading causes and brain response mechanisms to TBI damage.[3,4] Recent studies suggest the presence of cavitation in the human skull as a result of a TBI, which can arise due to the presence of small pockets of vapor in the cerebrospinal fluid (CSF).[5–10] Upon impact, these vapor contents expand and collapse due to a low pressure wave that reflects off the skull boundary after the initial compressive wave travels through the skull.[11] Cavitation has been proven to lead to significant erosion in alloys and hard plastics, applying a force that has been broadly characterized to a broad magnitude of 0.1–20 MPa.[12–16] Although the degree of cavitation exposure likely differs between varying applications, if cavitation has the ability to erode steel, its potential to cause damage on the surrounding brain tissue is alarming.

In this study, we investigate the topographical changes that cavitation induces to PDMS films to help illustrate the damage that cavitation has on brain tissue. Soft materials have been consistently used to model organs *in vitro* and in tissue engineering.[17] Soft polymers have been a common candidate for this as they are easy and affordable to manufacture, and their elastic properties can be easily altered and studied.[18] Adjusting the base to curing agent ratio in the PDMS fabrication process allows for arbitrary selection of the mechanical properties of PDMS.

The apparatus used to create cavitation on the PDMS films is similar to that used in previous studies.[19] This method is advantageous because it allows for controlled cavitation, enabling a similar cavitation exposure from one sample to the next. Characterization of cavitation aftermath is conducted using 3D confocal microscopy and interferometry methods. This analysis yields novelty in multiple research disciplines, like propulsion and hydrodynamic pumping, but in the TBI realm, it helps unmask the physical detriments that cavitation has on the nearby neuronal anatomy. Understanding this aftermath is a vital piece to advance TBI recovery, prevention, and care.

2. Experimental

2.1 PDMS fabrication and cavitation apparatus

PDMS samples were prepared by mixing the base and curing agent (Sylgard 184, Dow Corning, Midland, MI) at a 32 : 1 ratio and allowing them to cure at room temperature for 48 hours. Controlling the mass ratio of the base to curing agent affects the hardness of PDMS with higher ratios producing softer PDMS. The hardness of the PDMS samples is ~50 shore (PHT-960, Phase II, Upper Saddle River, NJ), which is comparable to that of the human brain which has been measured to be 10–30 shore in previous studies.[20] Also, the known elastic modulus of a similar PDMS sample measured at 560 kPa.[21] The known elastic modulus of a human brain ranges between 694 Pa (ref. 22) and

[a]*Department of Mechanical Engineering, Iowa State University, Ames, Iowa 50011, USA. E-mail: nastaran@iastate.edu*

[b]*Department of Biomedical Sciences, Iowa State University, Ames, IA 50011, USA*

9.2 kPa.[23] Each PDMS sample was collected and cured in a 36 mm Petri dish. The thickness of all the PDMS films was 3–6 mm.

The complete apparatus configuration followed closely the adhesion technique outlined in previous studies and is illustrated in Fig. 1.[7] This previously developed apparatus methodology is novel due to its level of control and efficiency in creating controlled cavitation. A 1.5 gallon tank is filled with deionized water and used to house the primary components of the apparatus. The PDMS-filled Petri dishes initially faced downward and were suspended mid-solution using a 3-axis stage (MT1, Thor Labs, Newton, New Jersey). Microbubbles (MBs) were produced by pushing air through a capillary tubing that had an inner diameter of 5 μm (Molex, Lisle, IL). The stream of rising MBs which was released from the tubing was oriented in the same plane as PDMS films. MBs exited the capillary tubing at a rate of ~75 MB per min. The adhered MBs for this study had a diameter of ~65 μm, similar to what is believed to exist *in vivo*, but altering capillary tubing size is directly correlated to the size of the outputted MBs.[3] Air was used to make the MBs in this study due to its similar composition to CSF.[7] For each trial, 450–500 MBs were collected across the exposed PDMS surface. The degree of cavitation presence *in vivo* is largely unknown; using 450–500 adhered MBs is a proof of concept and the amount of adhered MBs can arbitrarily be altered as *in vivo* cavitation is further researched and characterized. After MB collection, the PDMS sample was then moved out of plane with the rising MBs and rotated 180° so that it was exposed to an ultrasonic transducer, similar to the orientation shown in Fig. 1.[24] The activation of the transducer creates resonant conditions for the collected MBs and ultimately induces cavitation (100 kHz center frequency, 5 cycles, pulse repetition frequency 59 Hz, 260 V_{pp}). The necessary amplification of the transducer signal is generated through the implementation of a power amplifier (E&I, 1140LA). The process of collecting MBs, rotating the PDMS substrate, and inducing cavitation was done ten times for each sample. Control samples were submerged in the tank and exposed to the transducer signal but they did not have any adhered MBs, eliminating the occurrence of cavitation. The control samples experienced ultrasound exposure to ensure that any observed topographical differences were solely due to cavitation forces.

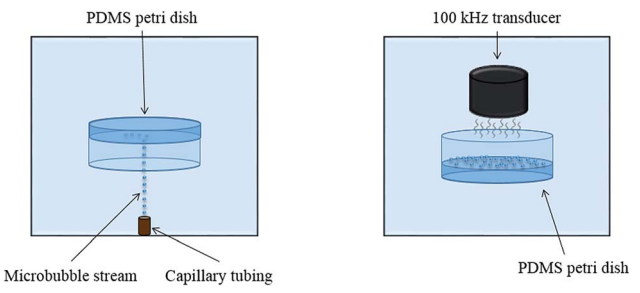

Fig. 1 Design apparatus for controlled cavitation simulation on PDMS films. MBs are initially collected on PDMS films when the Petri dish is directed downward. The Petri dish is then rotated 180° and exposed to an ultrasound transducer that induces dramatic MB oscillation, resulting in cavitation.

2.2 Topography analytics

Topographical analysis was conducted using 3D confocal microscopy and interferometry techniques (S neox, Sensofar, Barcelona, Spain). Compatible software (SensoSCAN v6.3) calculates roughness parameters that provide detailed characteristics of the sample topography. These parameters are useful when deciphering the difference between surface impurities, noise, and cavitation damage. All 3D confocal microscopy trials were conducted using a 150× objective lens, red light, and 60% lighting. Interferometry methods employed a 50XDi objective lens, green light, and 15% lighting. Both of these methods are used to legitimize topographical summaries of the PDMS surfaces on the nanoscale.

3. Results and discussion

3.1 3D confocal microscopy

The 3D confocal microscopy system has an assortment of capabilities and objective options. Fig. 2 represents a typical illustration of the surface of a control sample. Using a 150× objective lens condenses the dimensions of the field of view

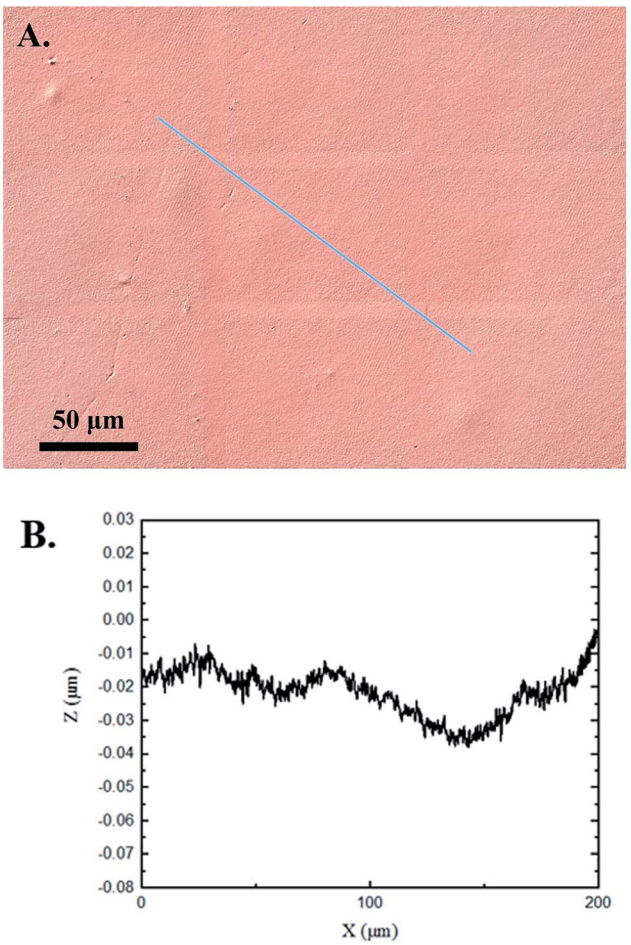

Fig. 2 3D confocal microscopy analysis of a control PDMS sample. (A) The surface is visibly flat with some minor surface impurities. (B) Graphical height displacement across an arbitrary line on the surface.

significantly. A stitched 3 × 3 field scan is implemented to collect data across a larger area and eliminate any bias from one particular region. Fig. 3 illustrates the typical topography of an experimental sample after experiencing the surrounding cavitation. A visual comparison yields distinct differences in the nature of the surface between the two samples. It appears that the cavitation has a created wear and erosion-like effects as small tears are visible on the surface of PDMS. This damage is consistently visually present in the experimental samples and absent in the control samples. The damage from cavitation is further elucidated through roughness parameters that are internally calculated in the software. The roughness parameter 'S_a' is used to portray the overall roughness of the surface by calculating the magnitude of the difference in height from the mean height. The S_a calculation gives an optimal description of the surface roughness due to the fact that in the derivation, impurities or foreign objects adhered to the surface have a minimal effect on the final value.[25] The average S_a value for all the control surfaces was calculated to be 22.0 nm. This value is noticeably different from the experimental samples, which had an average S_a value of 28.8 nm. This increase in roughness is expected due to the cavitation damage that is introduced.

The skewness (S_{sk}) is a dimensionless roughness parameter that also helps characterize the topography changes. A positive value of S_{sk} describes a height distribution that is below the mean plane, that is, the valleys create more of a bias than the peaks. A negative S_{sk} value resembles a bias toward the peaks in the sample. Our hypothesis was that cavitation would create cavities on the surface, yielding a positive S_{sk} value. Hypothetically the control samples would ideally have a S_{sk} value at or around zero, but this may slightly fluctuate due to natural impurities on the surface or minor ultrasound damage. The results align with our hypothesis with a control and experimental average S_{sk} value of 1.1 and 11.3, respectively. The positive S_{sk} value for the control sample is likely due to impurities that exist on the nanoscale during the curing process of PDMS.[26] The large S_{sk} value from the experimental samples points directly to an outside force creating erosion of the surface, similar to our anticipated hypothesis. This large S_{sk} also points to apparent cavitation damage because any debris or added noise that adheres to the surface by introducing the samples into the 1.5 gallon tank should cause a negative S_{sk} trend because they create peaks in the topography, but the cavitation erosion overrides this noise and remains biased below the mean height plane. Fig. 4 highlights the collected S_a and S_{sk} values from the control and experimental samples using 3D confocal microscopy. The *p*-values are also included to summarize the statistical significance of the data.

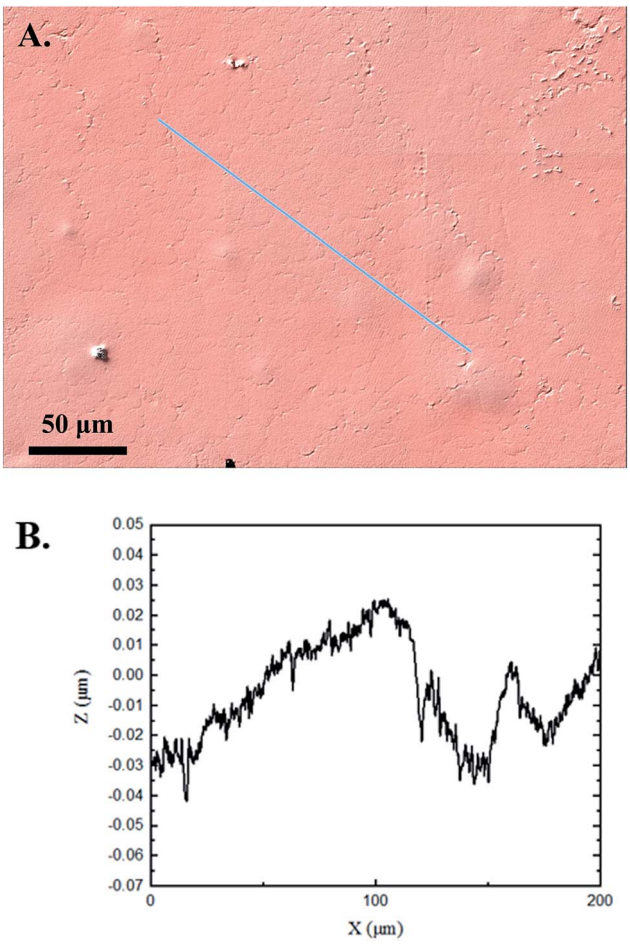

Fig. 3 3D confocal microscopy analysis of a typical experimental PDMS sample. (A) The surface shows patterns of wear which are distinct from the control visual. There appears to be some minor surface impurities. (B) Graphical height displacement across an arbitrary line on the surface.

3.2 Interferometry

Interferometry methods offer another optical method for investigating and upholding the differences shown between the control and experimental samples in the 3D confocal microscopy methods. Fig. 5 and 6 show illustrations of a typical control and experimental sample, respectively, *via* interferometry. Similar to 3D confocal microscopy, there is an apparent difference in the visual representation of the two surfaces. Noticeable wear and erosion are present on the experimental sample. Fig. 5B and 6B graphically represent the height of the surface along an arbitrary path. Both samples show noise and fluctuation in the surface height but only the experimental sample shows any sharp changes in the negative *z*-direction. This is significant because cavitation is theorized to cause nanoscale cavities with similar dimensions in other biomedical applications.[23] Any dust or debris added to the surface through the controlled cavitation process should show an additive height, not a subtractive difference. As a reminder, the control samples experience ultrasound exposure so this comparative data also eliminate the possibility of ultrasound being the primary contributor to the formation of these cavities. In essence, cavitation seems to be the only logical source of the resulting porous characteristics of the surface. Using interferometry techniques, the average S_a values for control and experimental samples are 45.7 nm and 90.0 nm, respectively. Additionally, the average S_{sk} value for the control samples is 0.3, compared to an average S_{sk} value of 5.3 for experimental samples. Fig. 7 summarizes the S_a and S_{sk} results from the control and experimental samples

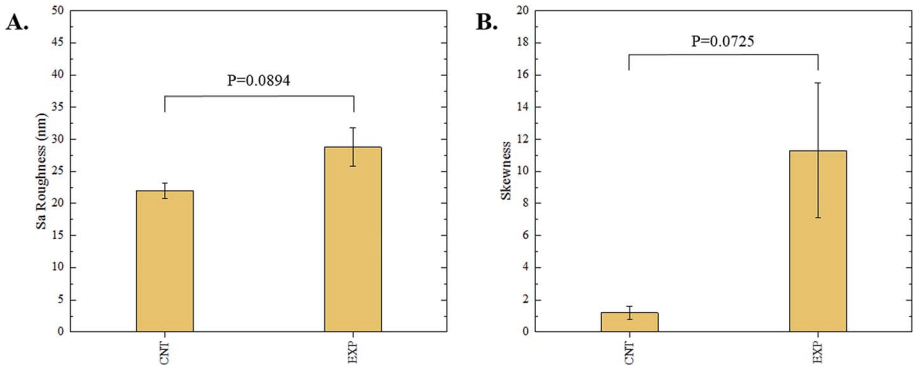

Fig. 4 Summary of (A) average S_a and (B) average S_{sk} roughness parameters of control and experimental samples *via* 3D confocal microscopy techniques. Error bars represent the standard error of the mean. $N = 5$.

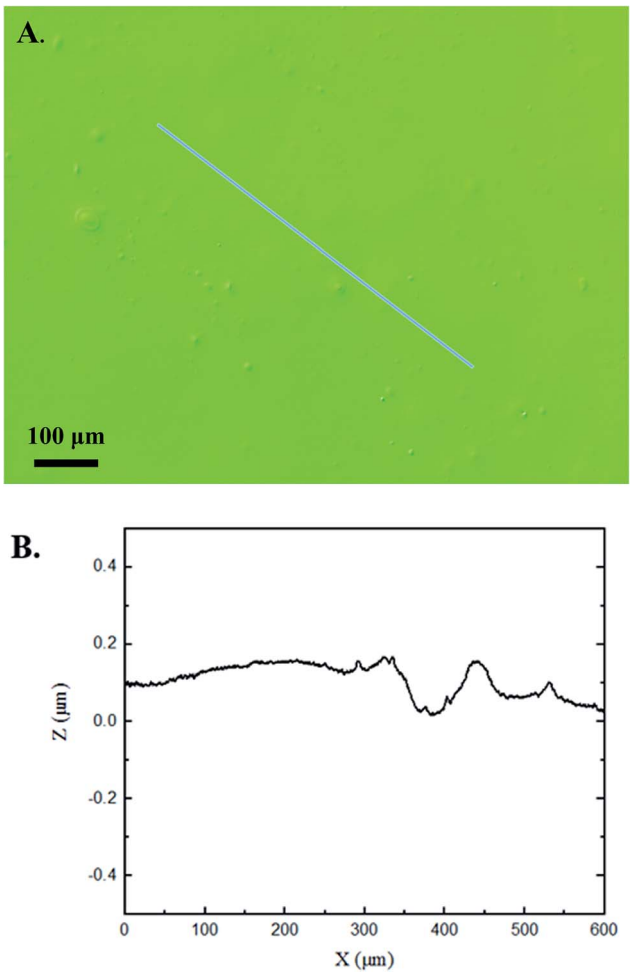

Fig. 5 Interferometry analysis of a control PDMS sample. (A) The surface is visibly flat with some minor surface impurities. (B) Graphical height displacement across an arbitrary line on the surface. Any abrupt spikes in the *z* direction appear to be above the surface.

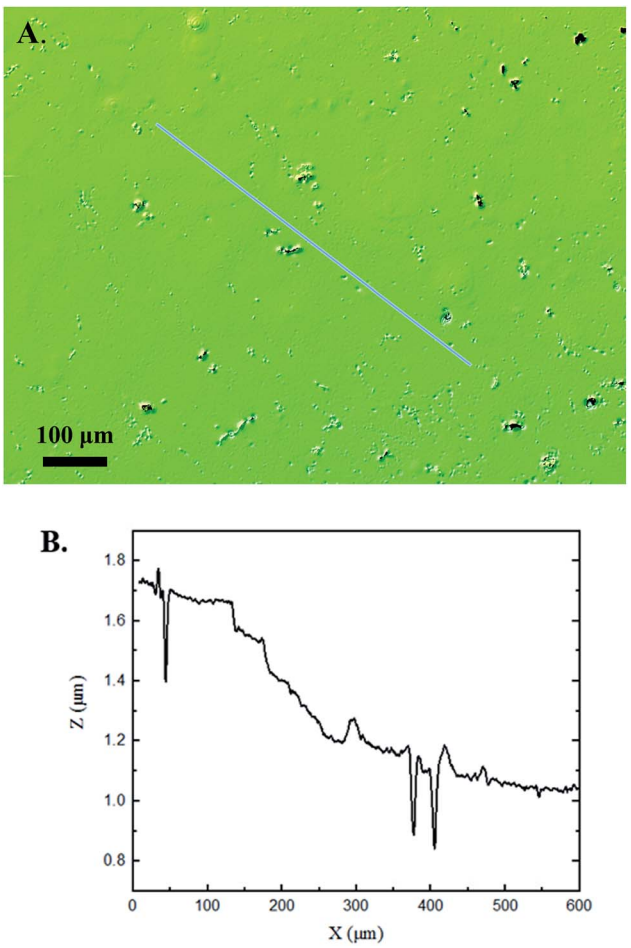

Fig. 6 Interferometry analysis of an experimental PDMS sample. (A) The surface has a roughness texture that is visually different from that in the control images. (B) The graphical height displacement across an arbitrary line on the surface shows abrupt spikes in the *z* direction below the surface, pointing to signs of cavitation damage.

using interferometry. The *p*-values are also included to summarize the statistical significance of the data. The large *p*-values for this application demonstrate that the topography is highly dependent on the degree of cavitation exposure that the field of view captures from one scan to the next. All in all, these trends demonstrate a rougher surface for experimental samples that have bias below the mean height plane, similar to the results from 3D confocal microscopy techniques.

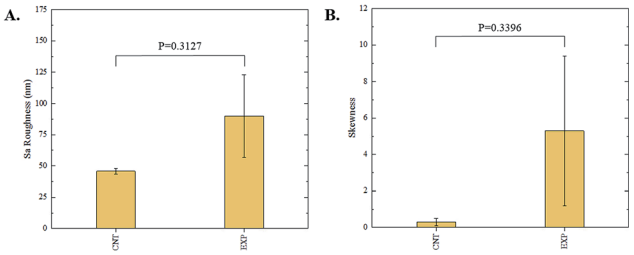

Fig. 7 Summary of (A) average S_a and (B) average S_{sk} roughness parameters of control and experimental samples *via* interferometry techniques. Error bars represent the standard error of the mean. $N = 5$.

Some experimental samples from both 3D confocal microscopy and interferometry yield similar roughness parameters compared to the mean values of the control samples, while others show distinct changes. This is likely due to the random positioning of MB adherence and induced cavitation, which lead to varied damage across the PDMS films, hence a larger standard error of the mean for experimental samples. Topographical analytics were collected randomly across the samples in order to eliminate visual bias. Additionally, to achieve nanoscale resolution, the field of view is 250 × 360 μm^2 and 680 × 980 μm^2 for 3D confocal microscopy and interferometry, respectively. This area is 54% and 403% of the average areal displacement between MBs on the surface, respectively. Because each area captures varying cavitation exposure, there is an expected increased discrepancy between individual surface scans. The overall trends point to clear topographical differences between the control and experimental samples using both 3D confocal microscopy and interferometry. This proven surface damage to a soft polymer with a slightly higher hardness and elastic modulus of the human brain offers great novelty, yet also brings about alarming awareness to the application of TBIs.

Characterizing the response of cranial anatomy to the surrounding cavitation is the next step for future studies. The resulting pressure field from the ultrasound beam was measured to be 60–100 kPa while inducing cavitation. This is important because brain damage is known to exist when the pressure exceeds a threshold of 173–235 kPa.[26] Using this apparatus in future biological testing confirms that any documented physical brain injury is primarily as a result of cavitation, not ultrasound exposure. Pharmacists can only provide the best treatment if the cellular response to this TBI phenomena is known. On top of this, if cellular damage shows catastrophic trends from cavitation exposure, then engineers now realize the importance of eliminating or minimizing the possibility of cavitation existence in helmet design. All in all, this study has demonstrated the detriments that cavitation has on soft surfaces and helped motivate the progression of TBI knowledge.

4. Conclusion

Cavitation is commonly known to exist and erode away nearby surfaces in a variety of applications, like propulsion and hydrodynamic pumping.[12,13,16] Recent theories have concluded that cavitation exists in the brain during a TBI and has the potential to leave behind detrimental effects.[5,6] This study uses an existing apparatus that simulates controlled cavitation and analyzes the damage that soft polymers undergo after exposure to the surrounding cavitation. Methods of 3D confocal microscopy and interferometry are used to study the surface topography of control and experimental samples. Comparative results conclude that induced cavitation leads to clear damage and erosion to a PDMS surface. Although the PDMS samples do not exactly replicate the damage that the human brain might experience, it is clear that damage occurs in our simulations and this raises concern for how detrimental cavitation is to vulnerable cranial anatomy. Future studies seek to focus on the response that neuronal cells have to similar simulations of controlled cavitation. Taken together, this study has clear novelty that helps unmask the highly unknown characteristics of TBIs, allowing for advancements in providing better care and treatment to its victims.

Conflicts of interest

There are no conflicts to declare.

Acknowledgements

The authors thank Timothy Bigelow for his help with ultrasound logistics and lending us a power amplification system. We also thank Curtis Mosher for his assistance and training with 3D confocal microscopy and interferometry. This work was supported by the Office of Naval Research (ONR) Grant N000141612246 and ONR Grant N000141712620.

References

1 A. Chanda, C. Callaway, C. Clifton and V. Unnikrishnan, *Mech. Adv. Mater. Struct.*, 2018, **25**, 1335–1341.
2 S. T. DeKosky, M. D. Ikonomovic and S. Gandy, *N. Engl. J. Med.*, 2010, **363**, 1293–1296.
3 J. L. Zamanian, L. Xu, L. C. Foo, N. Nouri, L. Zhou, R. G. Giffard and B. A. Barres, *J. Neurosci.*, 2012, **32**, 6391–6410.
4 S. Bartyczak and W. Mock, *J. Phys.: Conf. Ser.*, 2014, **500**, 182003.
5 J. Goeller, A. Wardlaw, D. Treichler, J. O'Bruba and G. Weiss, *J. Neurotrauma*, 2012, **29**, 1970–1981.
6 M. B. Panzer, B. S. Myers, B. P. Capehart and C. R. Bass, *Ann. Biomed. Eng.*, 2012, **40**, 1530–1544.
7 S. Haniff and P. A. Taylor, *Shock Waves*, 2017, **27**, 929–945.
8 H. Acar, S. Çınar, M. Thunga, M. R. Kessler, N. Hashemi and R. Montazami, *Adv. Funct. Mater.*, 2014, **24**, 4135–4143.
9 Y.-T. Wu and A. Adnan, *Sci. Rep.*, 2017, **7**, 5323.
10 W. Kang, A. Adnan, T. O'Shaughnessy and A. Bagchi, *Acta Biomater.*, 2018, **67**, 295–306.
11 P. A. Taylor, J. S. Ludwigsen and C. C. Ford, *Brain Injury*, 2014, **28**, 879–895.
12 B. Ji, X. Luo and Y. Wu, *J. Mech. Sci. Technol.*, 2014, **28**, 1339–1348.

13 B. K. Sreedhar, S. K. Albert and A. B. Pandit, *Wear*, 2017, **372–373**, 177–196.
14 M. Petkovšek and M. Dular, *Wear*, 2013, **300**, 55–64.
15 E. Herbert, S. Balibar and F. Caupin, *Phys. Rev. E: Stat., Nonlinear, Soft Matter Phys.*, 2006, **74**, 041603.
16 L. Chernin and D. V. Val, *Renewable Energy*, 2017, **113**, 688–696.
17 K. Y. Lee and D. J. Mooney, *Chem. Rev.*, 2001, **101**, 1869–1880.
18 M. Cabello, M. Mozo, B. D. la Cerda, C. Aracil, F. J. Diaz-Corrales, F. Perdigones, L. Valdes-Sanchez, I. Relimpio, S. S. Bhattacharya and J. M. Quero, *Sens. Actuators, B*, 2019, **288**, 337–346.
19 A. H. Wrede, A. Shah, M. C. McNamara, R. Montazami and N. N. Hashemi, *Ultrason. Sonochem.*, 2018, **43**, 114–119.
20 Z. Wang, A. A. Volinsky and N. D. Gallant, *J. Appl. Polym. Sci.*, 2014, **131**, 41050.
21 O. Clatz, H. Delingette, I. Talos, A. J. Golby, R. Kikinis, F. A. Jolesz, N. Ayache and S. K. Warfield, *IEEE Trans. Med. Imaging*, 2005, **24**, 1417–1427.
22 G. Soza, R. Grosso, C. Nimsky, P. Hastreiter, R. Fahlbusch and G. Greiner, *Int. J. Med. Robot Comp.*, 2005, **1**, 87–95.
23 Y. Zhou, K. Yang, J. Cui, J. Y. Ye and C. X. Deng, *J. Controlled Release*, 2012, **157**, 103–111.
24 E. S. Gadelmawla, M. M. Koura, T. M. A. Maksoud, I. M. Elewa and H. H. Soliman, *J. Mater. Process. Technol.*, 2002, **123**, 133–145.
25 C. Con and B. Cui, *Nanoscale Res. Lett.*, 2013, **8**, 394.
26 C. Ward, M. Chan and A. Nahum, Intracranial Pressure–A Brain Injury Criterion, *24th Stapp Car Crash Conference*, 1980, p. 24.